

See discussions, stats, and author profiles for this publication at: <https://www.researchgate.net/publication/259718827>

# Protein-Conjugated Quantum Dots Interface: Binding Kinetics and Label-Free Lipid Detection

ARTICLE *in* ANALYTICAL CHEMISTRY · JANUARY 2014

Impact Factor: 5.64 · DOI: 10.1021/ac403543g · Source: PubMed

---

CITATIONS

12

---

READS

98

## 6 AUTHORS, INCLUDING:



Md Azahar Ali

Iowa State University

38 PUBLICATIONS 356 CITATIONS

[SEE PROFILE](#)



Ved Varun Agrawal

National Physical Laboratory - India

54 PUBLICATIONS 772 CITATIONS

[SEE PROFILE](#)



Renu John

Indian Institute of Technology Hyderabad

46 PUBLICATIONS 757 CITATIONS

[SEE PROFILE](#)



Bansi Malhotra

Delhi Technological University

327 PUBLICATIONS 9,386 CITATIONS

[SEE PROFILE](#)

# Protein-Conjugated Quantum Dots Interface: Binding Kinetics and Label-Free Lipid Detection

Md. Azahar Ali,<sup>†,‡</sup> S. Srivastava,<sup>†</sup> M. K. Pandey,<sup>†</sup> Ved V. Agrawal,<sup>\*,†</sup> R. John,<sup>\*,‡</sup> and B. D. Malhotra<sup>\*,§</sup>

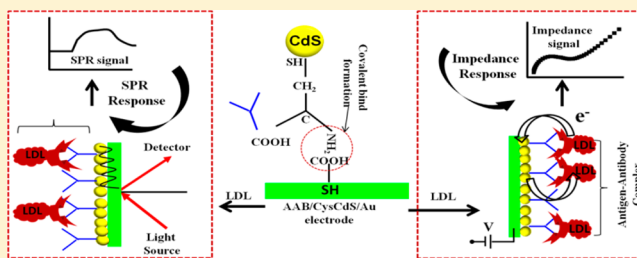
<sup>†</sup>Department of Science and Technology Centre on Biomolecular Electronics, Biomedical Instrumentation Section, CSIR-National Physical Laboratory, Dr. K. S. Krishnan Marg, New Delhi, Delhi 110012, India

<sup>‡</sup>Indian Institute of Technology Hyderabad, Ordnance Factory Estate, Yeddu-mailaram, Hyderabad, Andhra Pradesh 502205, India

<sup>§</sup>Department of Biotechnology, Delhi Technological University, Main Bawana Road, Shahbad Daulatpur, Delhi 110042, India

## Supporting Information

**ABSTRACT:** We propose a label-free biosensor platform to investigate the binding kinetics using antigen–antibody interaction via electrochemical and surface plasmon resonance (SPR) techniques. The L-cysteine in situ capped cadmium sulfide ( $\text{CdS}$ ; size  $< 7 \text{ nm}$ ) quantum dots (QDs) self-assembled on gold (Au) coated glass electrode have been covalently functionalized with apolipoprotein B-100 antibodies (AAB). This protein conjugated QDs-based electrode (AAB/CysCdS/Au) has been used to detect lipid (low density lipoprotein, LDL) biomolecules. The electrochemical impedimetric response of the AAB/CysCdS/Au biosensor shows higher sensitivity ( $32.8 \text{ k}\Omega \mu\text{M}^{-1}/\text{cm}^2$ ) in the detection range, 5–120 mg/dL. Besides this, efforts have been made to investigate the kinetics of antigen–antibody interactions at the CysCdS surface. The label-free SPR response of AAB/CysCdS/Au biosensor exhibits highly specific interaction to protein (LDL) with association constant of  $33.4 \text{ kM}^{-1} \text{ s}^{-1}$  indicating higher affinity toward LDL biomolecules and a dissociation constant of  $0.896 \text{ ms}^{-1}$ . The results of these studies prove the efficacy of the CysCdS-Au platform as a high throughput compact biosensing device for investigating biomolecular interactions.



Colloidal semiconductor quantum dots (QDs) have recently been projected for many applications including single cell labeling and imaging, tissue imaging, *in vivo* and *ex vivo* tumor imaging, assay labeling, fluorescence resonance electron transfer and biosensor development.<sup>1–3</sup> This has been possible because of the exceptional properties, such as the broad excitation spectra stretching into the ultraviolet region, narrow emission spectra, large Stokes shift, high resistance to photobleaching, stronger fluorescence, and excellent redox behavior, etc., associated with QDs.<sup>4</sup> The charge carriers (electrons/holes) in these QDs exhibit quantum confinement effect at room temperature and can be tuned by controlling their quantum yield.<sup>2</sup> The bioconjugation of these QDs can be achieved via covalent bond formation between QDs surface and desired biomolecules.<sup>5–7</sup> The conjugation of QDs can be easily achieved through cross-linking of carboxylic acid and amine ( $\text{COOH}-\text{NH}_2$ ) since these do not require any modification of the biomolecules (antibodies/oligonucleotides). Many approaches for capping and dispersion of  $\text{CdS}$  QDs have been investigated.<sup>8</sup> Xing et al. have compared characteristics of various QD-conjugation methods for immunohistochemical staining.<sup>9</sup> The tunable optical/electronic properties of cadmium sulfide ( $\text{CdS}$ ) and their surface hydrophilicity due to surface modification capabilities make them good candidates for detection of desired biomolecules.<sup>10</sup>

The numerous advantages of QDs combined with antibody–antigen specificity enable the development of QDs-based biosensors.<sup>11,12</sup> The  $\text{CdS}$  QDs can be used for both bioconjugation and amplification of the output signal leading to higher stability, sensitivity, and reliability of the desired biosensing devices.<sup>13,14</sup> Further,  $\text{CdS}$  QDs on Au substrate, by virtue of its desirable electrical properties may potentially facilitate identification of the biomolecules. Dhyani et al. have reported that the  $\text{CdS}$  QDs exhibit excellent redox activity because of higher charge detaching efficiency and synergetic effects.<sup>15</sup> Shen et al. have studied interaction between human adult hemoglobin (Hb) and  $\text{CdS}$  QDs using circular dichroism, fluorescence and Raman spectroscopic techniques under physiological pH.<sup>16</sup> It has been found that the presence of  $\text{CdS}$  QDs dramatically alters the conformation of Hb, quenched the intrinsic fluorescence of Hb, and decreases the  $\alpha$ -helix content of the secondary structure.<sup>16</sup>

The surface plasmon resonance (SPR) based biosensors have recently attracted much attention toward the development of diagnostic tools because of the ease of use, specificity, and high sensitivity to the target analyte, speed, capability for continuous monitoring, and multiplexing coupled with low-cost, portable

Received: October 29, 2013

Accepted: January 14, 2014

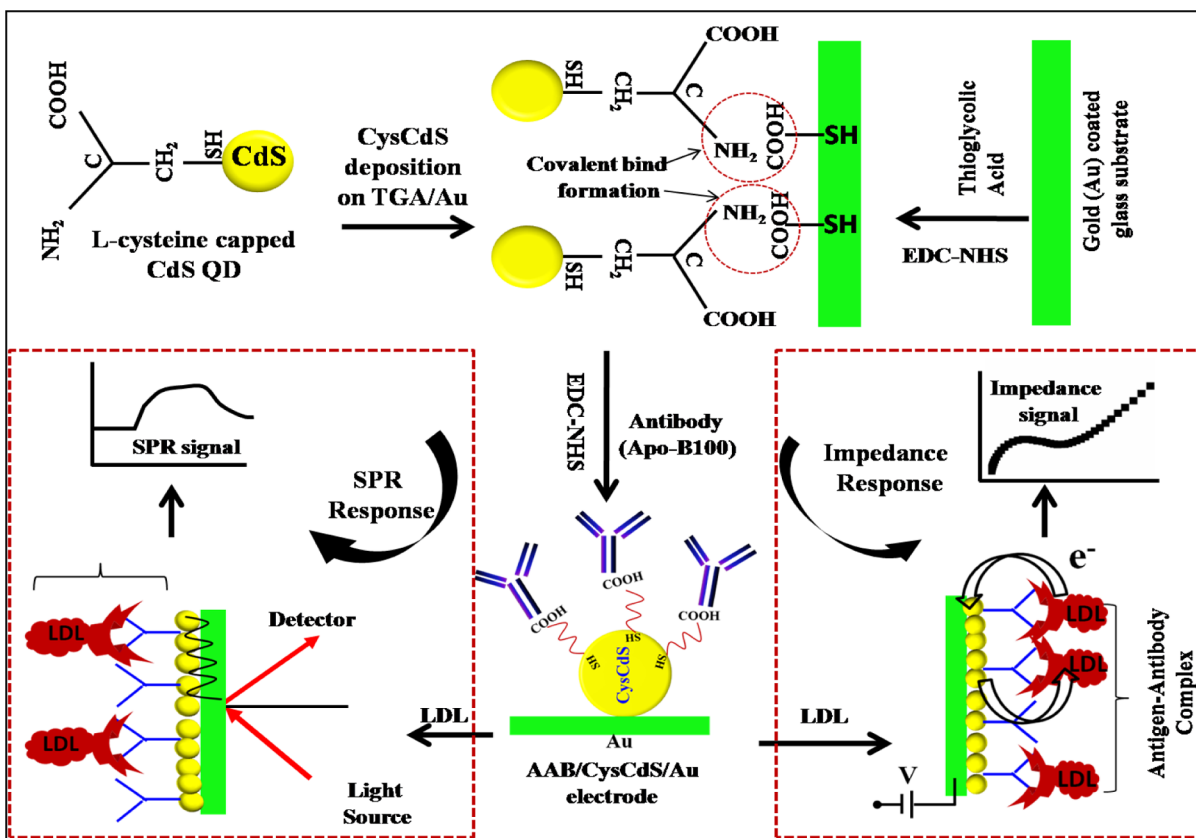
Published: January 14, 2014



ACS Publications

© 2014 American Chemical Society

**Scheme 1.** Schematic Representation of Apolipoprotein B100 (AAB) Functionalized CdS Quantum Dots Based Biosensor Platform for LDL Detection



instrumentation.<sup>17,18</sup> Xiao et al. have demonstrated a layer-by-layer surface decoration of QDs on gold (Au) substrate and investigated the interactions between the QDs and different proteins using *in situ* SPR technique.<sup>19</sup> Zayats et al. have reported photoelectrochemical properties of the Au-CdS nanoparticles array on a Au surface for detection of acetylcholine esterase using SPR spectroscopy.<sup>20</sup> Thus, Au-CdS QDs can be used to enhance the SPR signal resulting in higher sensitivity and selectivity for detection of antigen or biomolecules. The main advantage of the SPR system lies in its application for determination of both the affinity and binding kinetics of antibody–antigen interactions. Besides this, SPR allows real-time, rapid, and kinetics of noncovalent antibody–antigen interactions. By evaluation of the association/dissociation rates of the antibody–antigen interaction, antibodies with desired binding characteristics can be recognized. A fast association rate and a slow dissociation rate may result in the enhancement of immunosensor efficacy.

Attempts have recently been made toward the fabrication of biosensors for low density lipoprotein (LDL) detection.<sup>21</sup> Snellings et al. have modified the Au surface using dextran sulfate (DS) modified self-assembled monolayer (SAM) of 11-mercaptop-1-undecanol for detection of lipoprotein.<sup>22</sup> Matharu et al. have fabricated LDL sensor based on specific LDL-heparin interaction using SPR technique.<sup>23</sup> Jie et al. have utilized apolipoprotein B-LDL interaction for the fabrication of CdS nanocrystal based electroluminescence biosensor for LDL detection.<sup>24</sup> In spite of these developments, there is a considerable scope to fabricate LDL biosensors with improved characteristics.

It has recently been revealed that the cholesterol-enriched LDL in plasma can promote deposition of the plasma lipids in the artery wall and thereby elicit the formation of fatty streaks, atherosclerotic plaques, or both. The apolipoprotein B-100 (AAB) synthesized by the liver is known to act as a ligand for the LDL receptor on the surface of the liver cells. The mutations in LDL receptor or Apo B-100 may decrease the receptor-mediated uptake of LDL resulting in high level of LDL in plasma.<sup>21–28</sup> Friedewald et al. have reported that estimation of LDL-C concentration in plasma can be estimated by an indirect method without the use of preparative ultracentrifuging.<sup>29</sup> However, for general clinical applications, these methods require additional steps that are time-consuming.

In this paper, we demonstrate a label-free biosensor using self-assembled L-cysteine *in situ* capped CdS QDs on Au platform. The electrochemical impedance spectroscopy (EIS) and SPR techniques have been used to detect LDL using covalently conjugated protein (AAB) with L-cysteine capped CdS QDs on transducer surface. Besides this, the kinetic behavior of the antigen–antibody interactions has been evaluated using SPR technique.

## EXPERIMENTAL RESULTS

**Fabrication of QDs-Based Biosensing Platform.** The details of preparation of colloidal L-cysteine *in situ* capped CdS QDs have been described in the Supporting Information. To construct CdS QDs based biosensing platform, the Au plates are cleaned with acetone, ethanol and with copious amount of deionized water. Further, Au plates are treated with piranha solution ( $H_2SO_4/H_2O_2$ ; 7:3) for about 5 min followed by

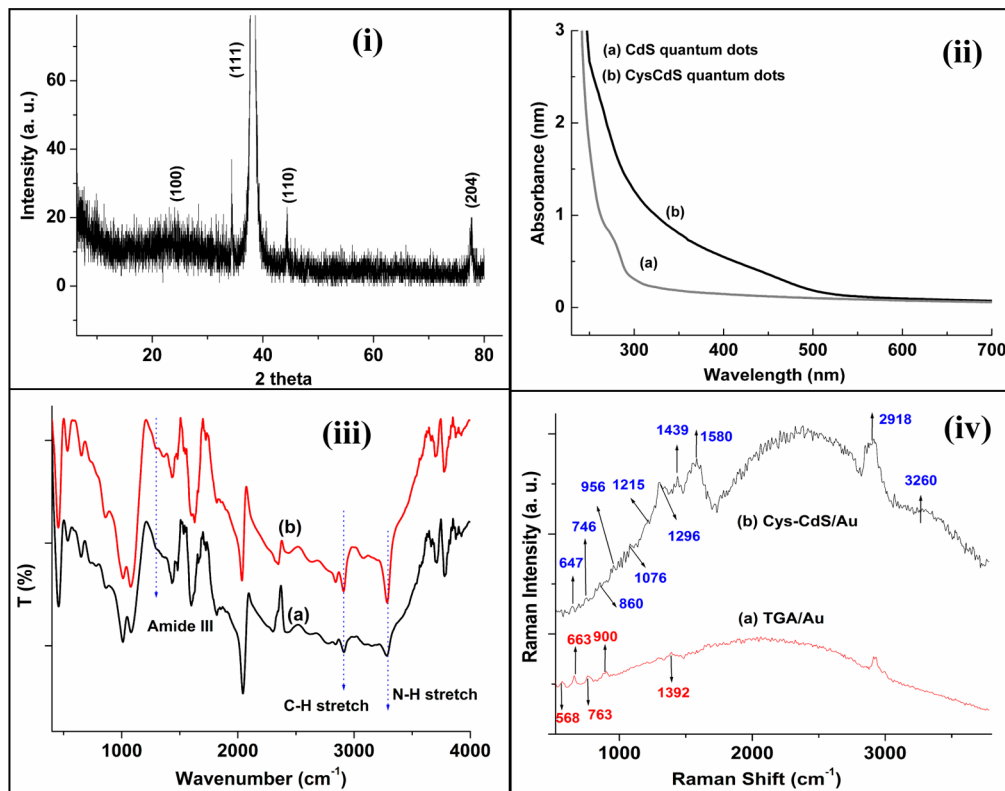


**Figure 1.** (i) X-ray diffraction pattern of CysCdS/Au film, (ii) UV-visible spectroscopy studies of synthesis CdS nanoparticles, (iii) FT-IR studies of different films, and (iv) Raman studies of (a) TGA/Au film and (b) CysCdS/Au film.

rinsing with deionized water and later with acetone and ethanol. The precleaned Au plate is then immersed into a 10 mM thioglycolic acid (TGA) solution for about 24 h at room temperature (25 °C) in dark conditions. The thiol (SH) group of TGA gets attached to Au surface via electrostatic interactions due to intrinsic property of Au which shows higher affinity toward Au surface. The Au plate is then washed with ethanol and acetone followed by deionized water to remove the TGA molecules. Again, the TGA/Au surface is used to treat EDC-NHS chemistry in which EDC (0.2 M) works as a coupling agent and NHS (0.05M) works as an activator. EDC-NHS activates the –COOH group in TGA. For SAM formation onto Au surface, the TGA/Au plate is dipped in L-cysteine in situ capped using CdS QDs solution for 4 h at room temperature under dark conditions.<sup>24</sup> The –NH<sub>2</sub> terminal of CysCdS quantum dots bind covalently with –COOH group of TGA and allow the formation of amide bond C–N. Again, the CysCdS/Au surface is treated for 4 h with EDC-NHS solution for activation of –COOH group of CysCdS. Then, AAB solution (1 mg/mL) is spread onto CysCdS/Au surface overnight in a humid chamber (at 4 °C) followed by washing with PBS containing 0.05% to remove any unbound AAB. This results in C–N bond formation between the –COOH group of CysCdS/Au and the –NH<sub>2</sub> terminal of AAB. Lastly, bovine serum albumin (BSA = 2 mg/dL) has been used for blocking the nonspecific adsorption of LDL (Scheme 1).

## ■ RESULTS AND DISCUSSION

**Structural Studies.** The results of X-ray diffraction (XRD) studies of the CysCdS/Au film shown in Figure 1i, indicate polycrystalline nature of the CysCdS film deposited onto Au substrate. The CdS QDs are known to exist in two forms

mainly the hexagonal (Wurtzite) and the cubic (Zincblend) crystalline structure. The presence of peaks with  $2\theta$  values at 24.8°, 43.3° and 77.7° may be associated with planes (100), (110), and (204), respectively [JCPDS (6-314)] indicating mixed hexagonal and cubic phase. The other reflection plane found at (111) pertains to the characteristic peak seen at 38.2° [JCPDS (65-2870)] and is due to the presence of Au on glass substrate.

The UV-visible spectra of CdS and CysCdS QDs are shown in Figure 1ii. In spectra a, absorption increases from 370 to 265 nm because of quantum confinement effect confirming the formation of CdS QDs. After L-cysteine modification, the absorption monotonically increases in the region, 492–200 nm [spectra b]. The radius ( $r$ ) of CysCdS quantum dots has been evaluated using the effective mass approximation model [eq 1].<sup>30</sup>

$$\Delta E = (\hbar^2 \pi^2 / 2R^2) \left( \frac{1}{m_e} + \frac{1}{m_h} \right) - \frac{1.8e^2}{\epsilon R} \quad (1)$$

where  $\Delta E$  is the increase in the band gap energy,  $\epsilon = 5.7$  is the relative dielectric constant, and  $m_e = 0.19m_0$  and  $m_h = 0.8m_0$  are the effective masses of electrons and holes, respectively. It has been found that the radius of CysCdS QDs is about 4–6 nm.

FT-IR spectra of the CysCdS/Au electrode (a) and AAB/CysCdS/Au bioelectrode (b) are shown in Figure 1iii. An intense peak at 1076 cm<sup>-1</sup> is assigned to C–O stretching because of the presence of the carboxylic group of TGA on Au surface. The intense peaks seen at 453 cm<sup>-1</sup> and 645 cm<sup>-1</sup> in the fingerprint region arise because of Cd–S bending (a). The peak observed at 2299 cm<sup>-1</sup> is attributed to S–H stretching resulting from thiol (–SH) complex with the core CdS quantum dot. The peaks found at 1600 and 1435 cm<sup>-1</sup> are due

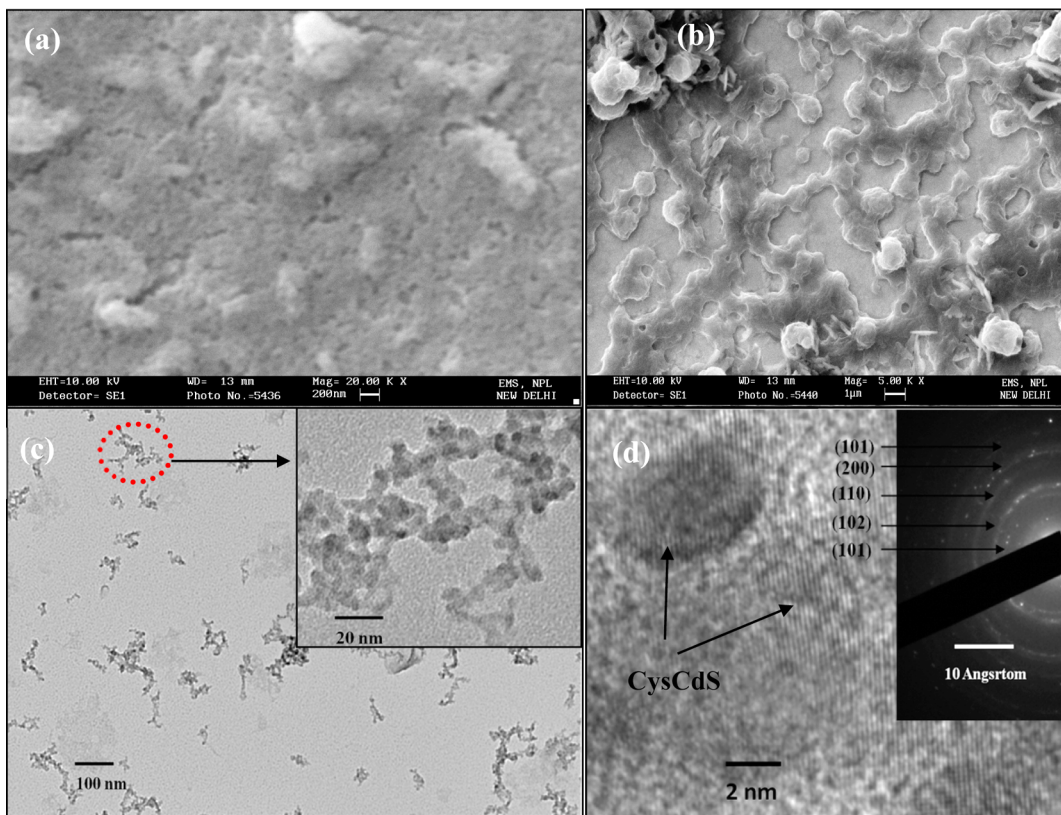


**Figure 2.** SEM studies of (a) CysCdS/Au, (b) AAB/CysCdS/Au, TEM analysis of (c) synthesis CysCdS nanoparticles (inset zoom image) and lattice fringes of CysCdS nanoparticles (d) (inset SAED pattern).

to amide bond II ( $-\text{NH}_2$ ) and  $-\text{COO}$  symmetric and unsymmetrical stretching induced by bonding of  $-\text{SH}$  with the core CdS. In the FT-IR spectra (b), intensity of the peak found at  $1600\text{ cm}^{-1}$  increases due to amide II ( $-\text{NH}_2$ ) stretching. This is attributed to antibody (AAB) and BSA functionalization onto CysCdS/Au surface and the peak at  $1427\text{ cm}^{-1}$  is shifted toward the lower wavenumber because of AAB incorporation. The stretching band found at  $1812\text{ cm}^{-1}$  in both spectra arising from  $\text{C=O}$  bond may be due to formation of CysCdS. The IR band found at  $2911\text{ cm}^{-1}$  is assigned to C–H stretching vibrations (asymmetric) of  $>\text{CH}_2$  of the AAB immobilized on CysCdS/Au surface (b). The intensity of  $>\text{CH}_2$  stretching vibration is found to be increased as compared to that of CysCdS/Au film. The peak intensity at  $3290\text{ cm}^{-1}$  corresponding to N–H stretch increases significantly in the case of AAB/CysCdS/Au electrode compared to that of CysCdS/Au film, because of the presence of amide A of the AAB molecules immobilized on the surface. In spectra b, an additional peak appearing at  $1300\text{ cm}^{-1}$  corresponds to amide III vibration. To confirm the presence of thiol in gold surface, we have investigated the Raman studies for TGA/Au (a) and CysCdS/Au (b) films (Figure 1iv). The Raman bands seen at  $763$  and  $663\text{ cm}^{-1}$  are assigned to the C–S stretching vibrations of adsorbed thiol molecules (a). The  $663\text{ cm}^{-1}$  band is attributed to the C–S stretching vibration for a gauche conformer of S–C–C chain, whereas the band at  $763\text{ cm}^{-1}$  is typical of a trans conformer.<sup>31</sup> More details of Raman studies are given in the Supporting Information.

**Contact Angle Studies.** The contact angle (CA) measurements have been carried out to delineate the hydrophilic/hydrophobic nature of the Au surface by sessile drop method

using a drop shape analyzer [Figure S1, Supporting Information]. The CA for the bare Au (image a) is found to be  $77^\circ$  indicating its hydrophobic nature. A CA of  $48^\circ$  measured at CysCdS/Au surface (image b) indicates the improved hydrophilicity of the modified surface. This is due to dominant hydrophilic property of L-cysteine modified CdS QDs that covalently bind with the Au surface thus reducing the hydrophobicity of the Au surface. After immobilization of AAB on CysCdS/Au (image c) surface, the value of CA decreases to  $38^\circ$  indicating improved hydrophilic nature of the Au surface which is attributed to the covalent attachment of AAB with CysCdS/Au.

**Morphological Studies.** Figure 2a and b show, respectively, the scanning electron micrograph (SEM) image of CysCdS/Au film before and after AAB functionalization. The CysCdS film (image a) with porous morphology structure gets agglomerated and appears as a bunch of CdS quantum dots. After antibody functionalization (image b), the surface shows a network-like structure. The agglomerated CdS QDs are coated with antibodies through strong covalent bond formation. The AAB functionalized CysCdS QDs appear as bunches of spherical structures that are connected to each other resulting in higher rough surface. This porous morphological structure of CysCdS can be used for AAB probing. The TEM image of the CysCdS QDs (Figure 2c) shows well-dispersed and uniformly distributed CdS QDs due to capping agent (L-cysteine) appearing as spherical in shape. The average size of the CysCdS QDs varies from 5 to 7 nm. The spherical structure of CysCdS QDs with the crystal lattice planes can be seen inside the boundaries of these spherical grains. Inset c shows the magnified image of CysCdS nanocrystals. It can be clearly seen

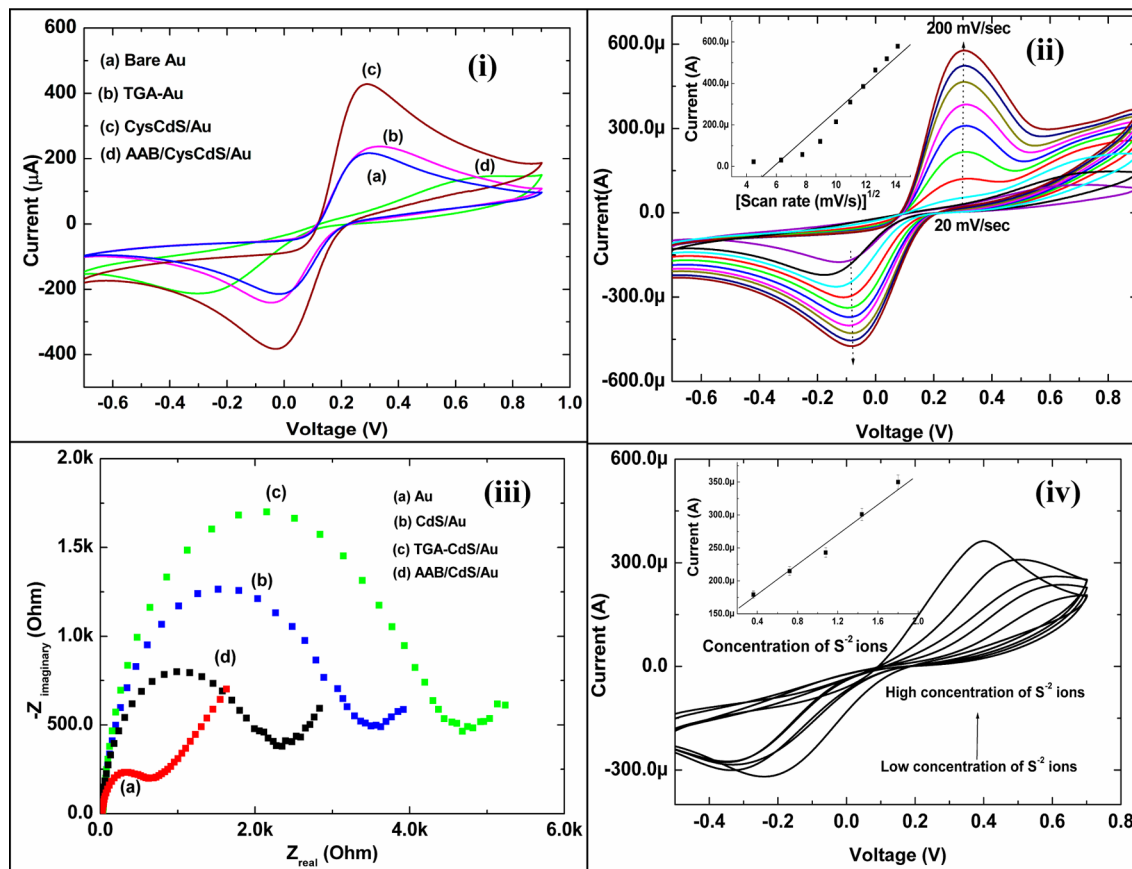


**Figure 3.** (i) Cyclic voltammogram (CV) of different electrodes in PBS solution (50 mM, pH 7.4, 0.9% NaCl) containing 5 mM  $[\text{Fe}(\text{CN})_6]^{3-/4-}$ , (ii) CV of AAB/CysCdS/Au bioelectrode as function of scan rate (20–200 mV/s) (inset anodic peak current vs root-mean-square of scan rate), (iii) electrochemical impedance spectroscopy (EIS) spectra of electrodes in PBS solution (50 mM, pH 7.4, 0.9% NaCl) containing 5 mM  $[\text{Fe}(\text{CN})_6]^{3-/4-}$ , and (iv) effects of different concentration of  $\text{S}^{2-}$  on Cd using CV (inset anodic current vs  $\text{S}^{2-}$  ions).

that the lattice fringes of CdS QDs arise due to its high crystalline structure (image d). The lattice spacing of CysCdS QDs is found to be as  $d_{110} = 0.205 \text{ nm}$  for the plane (110). The specific area electron diffraction (SAED) pattern of the CysCdS/Au electrode obtained from TEM studies (Figure 2d, inset) is in agreement with results of the XRD studies.

**Cyclic Voltammetry (CV) Studies.** CV studies have been carried out for different electrodes in the potential range, −0.7 V to +0.9 V vs Ag/AgCl (Figure 3i). Curve a shows well-defined oxidation and reduction peaks of bare Au electrode with peak-to-peak separation of 0.28 V. In the case of the thiolated Au electrode (curve b), after TGA treatment on Au surface, the peak current increases to 0.241 μA. The ratio of the cathodic to anodic current is close to 1, indicating quasi-reversible redox process at the electrode. The oxidation/reduction current of the CysCdS/Au electrode (curve c) is found to be higher compared to that of other electrodes. This is attributed to the fact that the CysCdS QDs act as a mediator and establish an electronic pathway to transport  $[\text{Fe}(\text{CN})_6]^{3-/4-}$  species toward the electrode leading to reduced tunnelling distance and good diffusion efficiency. After BSA and AAB immobilization onto CysCdS/ITO surface (curve d), the electrochemical current (or oxidation/reduction peaks) sharply decreases. This is because of the insulating properties of BSA and AAB molecules that perhaps obstruct (or impede) the acceleration of electrons and decrease mass transportation toward the electrode.

The surface charge density ( $Q_{\text{ads}}$ ) of BSA-antibodies adsorbed onto CysCdS/Au electrode has been calculated from the difference between the anodic oxidation and cathodic reduction charges in the presence of the adsorbing protein, after subtracting the small difference between these two charges in the absence of protein,<sup>32</sup> using eq 2

$$Q_{\text{ads}} = [Q_o^P - Q_r^P] - [Q_o - Q_r] \quad (2)$$

where  $Q_o^P$  and  $Q_r^P$  are the surface charge densities of anodic peak and cathodic peaks of AAB/CysCdS/Au, respectively, in the presence of protein.  $Q_o$  and  $Q_r$  are the surface charge densities of anodic peak cathodic peaks of CysCdS/Au, respectively. The surface concentration of proteins adsorbed (S) on CysCdS/Au electrode surface has been calculated to be  $3.48 \times 10^{-7} \text{ mol/cm}^2$  using  $Q_{\text{ads}} M_r / nF$ , where  $n$  is the number of electrons transferred (1),  $F$  is the Faraday constant (96 584 C/mol), and  $M_r$  is the molar mass of the protein. Jin et al. have reported the surface coverage of electroactive cytochrome c as 9.1 pmol·cm<sup>-2</sup> for mercaptoundecanoic acid modified p-Au electrode.<sup>33</sup> Thus, this CysCdS/Au platform provides a higher surface concentration due to incorporation of the CdS quantum dots.

Figure 3ii illustrates the CVs of AAB/CysCdS/Au bioelectrode with scan rate varying from 20 to 200 mVs<sup>-1</sup>. With increasing scan rates, there is an increase in both the cathodic and anodic peak currents with no shift in voltage, indicating a stable system. The inset in Figure 3ii shows the variation of anodic peak currents with the scan rate from 20 to 200 mVs<sup>-1</sup> revealing a surface controlled diffusion and quasi-reversible

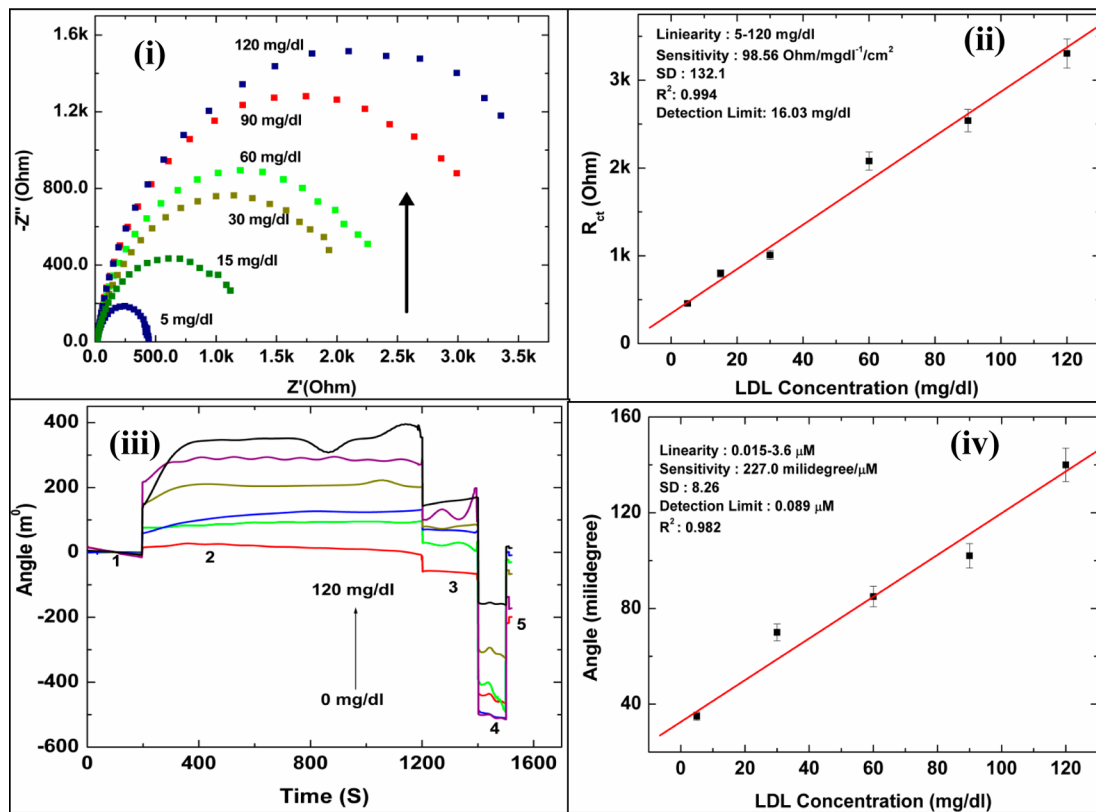


**Figure 4.** (i) EIS response of AAB/CysCdS/Au bioelectrode as a function of LDL concentrations (5–120 mg/dL) in PBS solution containing 5 mM  $[\text{Fe}(\text{CN})_6]^{3-/4-}$ , (ii) calibration plot between impedance response and different concentration of LDL, (iii) SPR response of AAB/CysCdS/Au bioelectrode as a function of LDL concentrations (5–120 mg/dL), 1-baseline, 2-association phase, 3-dissociation phase, 4-regeneration, and 5-baseline, and (iv) linear fit plot SPR angles vs LDL concentration.

process. The diffusivity of the AAB/CysCdS/Au bioelectrode in presence of redox species has been estimated to be  $7.45 \times 10^{-6}$  cm<sup>2</sup>/s using  $i_p = (269\,000)n^{3/2}AD^{1/2}Cr^{1/2}$  (Randles–Sevcik equation),<sup>28</sup> where  $i_p$  = redox peak current (A),  $n$  = number of electrons transferred in the redox event (1),  $A$  = electrode area (cm<sup>2</sup>),  $D$  = diffusion coefficient (cm<sup>2</sup>/s),  $C$  = surface concentration (mol/cm<sup>2</sup>),  $\nu$  = scan rate (mV/s). Mishra et al. have reported the diffusivity of ferrocyanide as  $6.3 \times 10^{-6}$  cm<sup>2</sup>/s for the antibody (human cardiac myoglobin) functionalized ZnS-rGO (ZnS nanocrystals decorated reduced graphene oxide) composite electrode.<sup>34</sup> The proposed AAB/CysCdS/Au bioelectrode provides comparable diffusivity of redox species as in literature.<sup>35</sup>

**Impedance Spectroscopy Studies.** EIS is versatile and efficient tool for observing the dynamics of antibody–antigen interactions. In EIS, the response of an electrochemical cell to a small amplitude sinusoidal AC signal as a function of frequency 0.01–10<sup>5</sup> Hz at a bias potential of 0.25 V. Electrical impedance ( $Z$ ) can be defined as the ratio of an incremental change in voltage  $V(t)$ , due to change in current  $I(t)$ , and is given by  $Z = (V(t))/(I(t)) = 1/Y = V_0 \sin(2\pi ft)/I_0 \sin(2\pi ft + \varphi)$ ,<sup>37</sup> where  $Y$  represents the complex conductance or admittance,  $V_0$  and  $I_0$  are the voltage and current (maximum), and  $t, f$ , and  $\varphi$  are the time, frequency, and phase shift between the voltage–time and current–time functions. The impedance can be described either by the modulus  $|Z|$  and the phase shift  $\varphi$  or by the real part ( $Z'$ ) and the imaginary part ( $Z''$ ) of the signal through Nyquist plot representation. The simplest and most frequently used equivalent circuit for modeling the EIS experimental data is the Randles circuit (Scheme S1b, Supporting Information), that

comprises of the electrolyte ( $R_s$ ), in series with the capacitance of the dielectric layer ( $C_{dl}$ ), the charge-transfer resistance ( $R_{ct}$ ), and the Warburg impedance ( $Z_w$ ). A typical shape of Nyquist plot includes a semicircle region lying on the real axis followed by a straight line. The linear part ( $\psi = \pi/4$ ), observed in the low frequency range, indicates a mass-transfer limited process, where the semicircle portion indicates a charge-transfer limited process, observed in the high frequency range (Scheme S1a, Supporting Information). The imaginary component, at high frequency falls to zero because it offers no impedance. The capacitance  $C_{dl}$  offers high impedance as the frequency drops and hence, the current flows mostly through  $R_{ct}$  and  $R_s$ . The double layer capacitance or constant phase element (CPE) can be calculated from the frequency at the maximum of the semicircle ( $\omega = 2f = 1/R_{ct}C_{dl}$ ). The charge-transfer resistance  $R_{ct}$  and the double layer capacitance  $C_{dl}$  are the most important electrical parameters for analyses of the change in impedance for antibody–antigen interactions. The parameter of interest here is  $R_{ct}$  that can be extracted from the fitted circuit model. Figure 3iii shows the  $R_{ct}$  value of the CysCdS/Au (c) as 1.99 k $\Omega$ , which is low compared to that of the bare Au (a) and TGA/Au electrodes (b). This is because CdS QDs act as a mediator for electron transfer and reduce the electron tunnelling distance from the redox probe  $[\text{Fe}(\text{CN})_6]^{3-/4-}$  in bulk solution to electrode resulting in a decrease of  $R_{ct}$ . The increased  $C_{dl}$  of AAB/CysCdS/Au (18.2  $\mu\text{F}$ ) compared to that of CysCdS/Au (7.04  $\mu\text{F}$ ) is because of the presence of AAB molecules that have been prepared in PBS containing 150 mM NaCl. The presence of the salt may increase the  $C_{dl}$  value as the reported literature.<sup>36</sup> After AAB immobilization onto CysCdS/

Au surface, the  $R_{ct}$  value increases to 3.34 k $\Omega$  (Table S1, Supporting Information). This is attributed to the antibody (AAB)–CysCdS interaction which impedes the transfer of ions from bulk solution to electrode or antibody and BSA acts as an insulating material which covalently binds with CysCdS resulting in blocking of charge transfer through the diffusion layer. The presence of bulky protein molecules causes steric hindrance to the electron transfer.

**Effect of S<sup>2-</sup> Ions on CysCdS/Au Electrode.** The electrochemical properties of CysCdS/Au electrodes have been investigated by varying the concentration of S<sup>2-</sup> ions or Na<sub>2</sub>S precursor during *in situ* synthesis of CysCdS using CV and EIS techniques. It has been found that magnitude of current using CV studies increases on adding S<sup>2-</sup> ions [Figure 3iv], indicating increased current dependence on concentration of the S<sup>2-</sup> ions. This may be due to adsorption of S<sup>2-</sup> ions onto the CysCdS surface. The CysCdS/Au electrode with higher concentration of S<sup>2-</sup> ions exhibits good catalytic redox behavior. Yang et al. have reported sulfur-doped graphene as an efficient metal-free cathode catalyst for oxygen reduction.<sup>37</sup> The similar results are observed using EIS studies, wherein the  $R_{ct}$  value decreases linearly with increasing S<sup>2-</sup> ions concentration (Figure S2i and ii, Supporting Information). This is attributed to increased accumulation of S<sup>2-</sup> ions on electrode surface resulting in enhanced  $[\text{Fe}(\text{CN})_6]^{3-/4-}$  redox species toward electrode leading to decreased  $R_{ct}$ . Besides this, the  $C_{dl}$  value between the electrode and electrolyte has been found to increase with increased S<sup>2-</sup> concentration (Table S2, Supporting Information). This optimized concentration of CysCdS based electrode has been used for biosensing.

**Impedimetric Response Studies.** The impedimetric response for the AAB/CysCdS/Au bioelectrode as a function of lipid (LDL) concentration (5–120 mg/dL) with an incubation time of about 5 min is obtained from the Nyquist plots (Figure 4i). The change in  $R_{ct}$  value or dielectric/blocking properties of the AAB/CysCdS/Au bioelectrode arises because of antigen–antibody interaction at electrode/electrolyte interface. It can be seen that the  $R_{ct}$  value increases linearly for the AAB/CysCdS/Au bioelectrode on addition of LDL concentration (Figure 4ii). Higher  $R_{ct}$  value indicates that the presence of the insulating layer of LDL onto AAB/CysCdS/Au bioelectrode surface inhibits penetration of the redox species toward the electrode, resulting in higher diameter of EIS spectra and lower charge transfer rate constant. The negative charge carried by the LDL molecules perhaps blocks the electron transfer of the  $[\text{Fe}(\text{CN})_6]^{3-/4-}$  redox couple resulting in higher impedance. The bioelectrode when treated with 0.2 M glycine solution of pH 2.4 for about two minutes results in 95% of the regeneration of the bioelectrode. The plot between  $R_{ct}$  value and LDL concentration (5–120 mg/dL) yields  $R_{CT}(\Omega) = 384.4(\Omega) + 24.6 \Omega \text{ mg dL}^{-1} \times \text{LDL concentration}$ . The sensitivity of this AAB/CysCdS/Au bioelectrode is found to be as high as 32.8 k $\Omega \mu\text{M}^{-1}/\text{cm}^2$  (Table S3, Supporting Information) with regression coefficient ( $r^2$ ) as 0.994. It has been found that this impedimetric biosensor sensor exhibits a low detection limit of 16.03 mg/dL. In Supporting Information Table S3, compared to other reported biosensors,<sup>23,38</sup> the proposed biosensor shows a low detection limit and is capable of detecting LDL (up to 120 mg/dL) in the physiological range of LDL human blood. This AAB/CysCdS/Au biosensor exhibits a good linearity as 5–120 mg/dL as compared to that in the literature.<sup>23,38</sup>

**SPR Studies.** Figure S3 (Supporting Information) shows SPR spectra of the self-assembled CysCdS onto Au disc with AAB functionalization before a and after b. The surface plasmon angle shifts to higher value (from 0.043 to 0.288 millidegree) after AAB functionalization on CysCdS/Au surface. The SPR response of the AAB/CysCdS/Au biosensor has been studied at room temperature (298 K) using PBS solution (50 mM, pH 7.4, 150 mM NaCl) as a function LDL concentration. The excess lipid (LDL) solution is removed after completion of binding time and then, the buffer is injected again to the cuvette using automatic sequence to bring identical conditions prior to the binding phase. The difference in the SPR angle before and after the binding phase has been utilized to analyze the binding of LDL with AAB/CysCdS/Au bioelectrode. Figure 4iii shows typical SPR sensogram obtained for the AAB/CysCdS/Au bioelectrode in presence of various LDL concentrations. The time dependent increment in the SPR angle during association indicates successful binding of LDL onto AAB/CysCdS/Au surface. The calibration plot of the change in angle ( $\Delta m^\circ$ ) vs LDL concentration exhibits increase in the SPR angle with increasing LDL concentration [Figure 4iv]. The linearity of this SPR is obtained in the range, 5–120 mg/dL with regression coefficient ( $r^2$ ) of 0.982 and standard deviation as 8.26. This fabricated AAB/CysCdS/Au biosensor can be used to quantify LDL in the physiological range (<120 mg/dL). The sensitivity of the AAB/CysCdS/Au biosensor has been calculated to be as  $290.0 m^\circ \mu\text{M}^{-1}$  from the calibration curve with a lower detection limit of 0.08  $\mu\text{M}$ .

**Kinetic Analysis of AAB–LDL Interaction.** The kinetic analysis of the AAB–LDL interaction has been investigated using SPR at room temperature (298 K). The nonlinear curve fitting has been performed to evaluate the association phase during binding using kinetics evaluation software. The binding reaction equation for the two macromolecular interactants is  $[A] + [B] \rightleftharpoons [AB]$ .<sup>23</sup> The rate of formation of complex in association phase, is given by<sup>23</sup>

$$\frac{d[AB]}{dt} = K_a[A][B] - k_d[AB] \quad (3)$$

The integrated rate equation for associated phase is given as

$$R_t = \frac{k_a C R_{\max}}{k_a C + k_d} (1 - e^{-(k_a C + k_d)t}) + R_0$$

$$\text{or } R_t = E(1 - e^{-k_s t}) + R_0 \quad (4)$$

where  $K_a$  is the association rate constant,  $k_d$  is the dissociation rate constant,  $R_0$  represent the signal at zero time, and  $(k_a C R_{\max})/(k_a C + k_d)$  is maximal of change in the response. The relevant kinetic information is obtained from  $k_s = k_a C + k_d$ . The  $k_a$  and  $k_d$  are evaluated from the plot of  $k_s$  versus C (LDL concentration) where slope of curve gives the value of  $k_a$  and y-intercept gives the information about  $k_d$ . The observed values of  $k_a$  and  $k_d$  rate constants for AAB–LDL binding are estimated to be  $33.4 \times 10^3 \text{ M}^{-1} \text{ s}^{-1}$  and  $8.96 \times 10^{-2} \text{ s}^{-1}$ , respectively, with the equilibrium constant for association ( $K_A = k_a/k_d$ ) as  $3.7 \times 10^5 \text{ M}^{-1}$ . The proposed biosensor shows higher  $k_a$  and  $k_d$  values compared to those obtained using SAM of 4-aminothiophenol of Au substrate ( $0.0967 \text{ kM}^{-1} \text{ s}^{-1}$  and  $2.64 \times 10^{-4} \text{ s}^{-1}$ ).<sup>23</sup>

**Selectivity and Stability Studies.** To determine specificity of the AAB/CysCdS/Au electrode toward LDL (60 mg/dL) detection, the effect of analytes, such as free cholesterol (150 mg/dL), cholestryloleate (150 mg/dL) and triglyceride (150 mg/dL) has been investigated using EIS technique in similar

conditions as used for LDL detection (Figure S4i, Supporting Information). The results reveal that there is negligible change (reduced 98.99%) in the impedance signal in presence of these analytes indicating non-interference. These results indicate that the AAB/CysCdS/Au electrode shows high selectivity toward LDL detection as is evident by low relative standard deviation (RSD) 0.43% ( $n = 5$ ).

The storage stability of the AAB/CysCdS/ITO bioelectrode has been determined by observing the  $R_{ct}$  value at regular intervals of time for 90 days. The AAB/CysCdS/ITO bioelectrode is stored at 40 °C when not in use. The bioelectrode is found to exhibit 95% response up to about 42 days after which the  $R_{ct}$  value decreases and reaches 85% of  $R_{ct}$  in 90 days with RSD value of 5.8% ( $n = 12$ ) (Figure S4ii, Supporting Information).

**Reproducibility Studies.** The reproducibility of the AAB/CysCdS/ITO biosensor has been conducted using EIS technique for different working electrodes under the same set of conditions with concentration of LDL (60 mg/dL) (Figure S4iii, Supporting Information). It has been found that this biosensor shows good reproducibility for different electrodes (five) with constant sensor surface area as evidenced by the relative standard deviation (RSD) of 0.55% (mean value = 2.09 kΩ). The low RSD (0.55%) of this fabricated AAB/CysCdS/ITO biosensor indicates good precision.

## CONCLUSION

In summary, a novel biosensor based on protein (AAB) functionalized CysCdS on gold substrate has been fabricated to evaluate the antigen–antibody binding kinetics for lipid (LDL) detection via EIS and SPR techniques. The electrochemical performance of the proposed CysCdS/ITO electrode has been investigated by tuning the  $S^{2-}$  ions (sulfur) during CysCdS formation. The observed higher value of association and dissociation rate constants of AAB-LDL binding reveal strong affinity between CysCdS functionalized AAB and LDL molecule. The electrochemical properties of fabricated CysCdS/Au electrode can be controlled by varying concentration of  $S^{2-}$  ions during *in situ* synthesis of CysCdS. The AAB/CysCdS/Au electrode shows a good selectivity for LDL detection and exhibits detection range as 5–120 mg/dL within the physiological range of LDL in blood/serum. The CysCdS QDs provide a biocompatible and favorable environment because of high surface-to-volume ratio resulting in enhanced loading capacity of AAB. This AAB/CysCdS/Au biosensor shows higher sensitivity as 32.8 kΩ  $\mu M^{-1}/cm^2$  (impedance) or 290.0  $m^{\circ} \mu M^{-1}$  (SPR) and fast response. The application of self-assembled CysCdS QDs not only improves the electrochemical conduction behavior of this biosensor but also results in enhanced SPR angle change. The high sensitivity combined with specificity of LDL–AAB binding, toward LDL detection using CysCdS nanocrystals is a potential platform that can be used to detect other lipids, such as VLDL, triglycerides, etc.

## ASSOCIATED CONTENT

### Supporting Information

Additional information as described in the text. This material is available free of charge via the Internet at <http://pubs.acs.org>.

## AUTHOR INFORMATION

### Corresponding Authors

\*E-mail: ved.varun@gmail.com.

\*E-mail: renujohn@iith.ac.in.

\*E-mail: bansi.malhotra@gmail.com. Phone: 91-11-27871043 (Ext-1609). Fax: 91-11-27871023.

### Author Contributions

M.A.A. and S.S. contributed equally.

### Notes

The authors declare no competing financial interest.

## ACKNOWLEDGMENTS

We thank Director NPL, New Delhi, India for the facilities. Md.A.A. and S.S. are thankful to CSIR, for the award of Senior Research Fellowships. Authors are thankful to the Advance Instrumentation and Research Facilities (AIRF) and Mr. Hemant Dhyani, JNU, New Delhi for TEM studies. V.V.A. is thankful to CSIR Empower project for funding. The financial support received from Department of Science and Technology, India (Grant No. DST/TSG/ME/2008/18), and Indian Council of Medical Research, India (Grant No. ICMR/5/3/8/91/GM/2010-RHN) is gratefully acknowledged.

## REFERENCES

- (1) Bruchez, M., Jr.; Moronne, M.; Gin, P.; Weiss, S.; Alivisatos, A. P. *Science* **1998**, *281*, 2013–2015.
- (2) Gao, X.; Cui, Y.; Levenson, R. M.; Chung, L. W. K.; Nie, S. *Nat. Biotechnol.* **2004**, *22*, 969–976.
- (3) Dennis, A. M.; Rhee, W. J.; Sotto, D.; Dublin, S. N.; Bao, G. *ACS Nano* **2012**, *4*, 2917–2924.
- (4) Chan, W. C. W.; Maxwell, D. J.; Gao, X. H.; Bailey, R. E.; Han, M. Y.; Nie, S. M. *Curr. Opin. Biotechnol.* **2002**, *13*, 40–46.
- (5) Chan, W. C. W.; Nie, S. M. *Science* **1998**, *281*, 2016–2018.
- (6) Mattossi, H. *J. Am. Chem. Soc.* **2000**, *122*, 12142–12150.
- (7) Jaiswal, J. K.; Mattossi, H.; Mauro, J. M.; Simon, S. M. *Nat. Biotechnol.* **2003**, *21*, 47–51.
- (8) Li, H.; Shih, W. Y.; Shih, W.-H. *Ind. Eng. Chem. Res.* **2007**, *46*, 2013–2019.
- (9) Xing, Y.; Chaudry, Q.; Shen, C.; Kong, K. Y.; Zhou, H. E.; Chung, L. W.; Petros, J. A.; O'Regan, R. M.; Yezhelyev, M. V.; Simons, J. W.; Wang, M. D.; Nie, S. *Nat. Protoc.* **2007**, *2*, 1152–1165.
- (10) Medintz, L. I.; Uyeda, H. T.; Goldman, E. R.; Mattossi, H. *Nat. Mater.* **2005**, *4*, 435–446.
- (11) Mani, V.; Chikkaveeraiah, B. V.; Patel, V.; Gutkind, J. S.; Rusling, J. F. *ACS Nano* **2009**, *3*, 585–594.
- (12) Chikkaveeraiah, B. V.; Bhirde, A. A.; Morgan, N. Y.; Eden, H. S.; Chen, X. *ACS Nano* **2012**, *6*, 6546–6561.
- (13) Wang, K.; Liu, Q.; Guan, Q.-M.; Wu, J.; Li, H.-N.; Yan, J.-J. *Biosen. Bioelectron.* **2011**, *26*, 2252–2257.
- (14) Huang, Y.; Zhang, W.; Xiao, H.; Li, G. *Biosen. Bioelectron.* **2005**, *21*, 817–821.
- (15) Dhyani, H.; Ali, Md. A.; Pandey, M. K.; Malhotra, B. D.; Sen, P. *J. Mater. Chem.* **2012**, *22*, 4970.
- (16) Shen, X.-C.; Liou, X.-Y.; Ye, L.-P.; Liang, H.; Wang, Z.-Y. *J. Colloid Interface Sci.* **2007**, *15*, 400–6.
- (17) Hotta, K.; Yamaguchi, A.; Teramae, N. *ACS Nano* **2012**, *6*, 1541–1547.
- (18) Fujii, E.; Koike, T.; Nakamura, K.; Sasaki, S.; Kurihara, K.; Citterio, D.; Iwasaki, Y.; Niwa, O.; Suzuki, K. *Anal. Chem.* **2002**, *74*, 6106–6110.
- (19) Xiao, Q.; Zhou, B.; Huang, S.; Tian, F.; Guan, H.; Ge, Y.; Liu, X.; He, Z.; Liu, Y. *Nanotechnology* **2009**, *20*, 325101.
- (20) Zayats, M.; Kharitonov, A. B.; Pogorelova, S. P.; Lioubashevski, O.; Katz, E.; Willner, I. *J. Am. Chem. Soc.* **2003**, *125*, 16006–16014.
- (21) Yan, W.; Chen, X.; Li, X.; Feng, X.; Zhu, J.-J. *J. Phys. Chem. B* **2008**, *112*, 1275–1281.
- (22) Snellings, S.; Fuller, J.; Pitner, M.; Paul, D. W. *Biosens. Bioelectron.* **2003**, *19*, 353–363.
- (23) Matharu, Z.; Arya, S. K.; Sumana, G.; Gupta, V.; Malhotra, B. D. *J. Mol. Recognit.* **2008**, *21*, 419–424.

- (24) Jie, G.; Liu, B.; Pan, H.; Zhu, J.; Chen, H. *Anal. Chem.* **2007**, *79*, 5574–5581.
- (25) Martin, S. P.; Lamb, D. J.; Lynch, J. M.; Reddy, S. M. *Anal. Chim. Acta* **2003**, *487*, 91–100.
- (26) Gaus, K.; Hall, E. A. H. *J. Colloid Interface Sci.* **1999**, *217*, 111–118.
- (27) Gaus, K.; Hall, E. A. H. *Anal. Chim. Acta* **2002**, *470*, 3–17.
- (28) Ali, Md. A.; Srivastava, S.; Solanki, P. R.; Agrawal, V. V.; John, R.; Malhotra, B. D. *Appl. Phys. Lett.* **2012**, *101*, No. 084105.
- (29) Friedewald, W. T.; Levy, R. I.; Fredrickson, D. S. *Clin. Chem.* **1972**, *18*, 499–502.
- (30) Einevoll, G. T. *Phys. Rev. B* **1992**, *45*, 3410–3417.
- (31) Królikowska, A.; Kudelski, A.; Michota, A.; Bukowska, J. *Surf. Sci.* **2003**, *10*, 227–232.
- (32) Wright, J. E.I.; Cosman, N. P.; Fatih, K.; Omanovic, S.; Roscoe, S. G. *J. Electroanal. Chem.* **2004**, *564*, 185–197.
- (33) Jin, B.; Wang, G.-X.; Millo, D.; Hildebrandt, P.; Xia, X.-H. *J. Phys. Chem. C* **2012**, *116*, 13038–13044.
- (34) Mishra, S. K.; Srivastava, A. K.; Kumar, D.; Biradar, A. M.; Rajesh. *Nanoscale* **2013**, *5*, 10494.
- (35) Chang, B.-Y.; Park, S.-M. *Annu. Rev. Anal. Chem.* **2010**, *3*, 207–29.
- (36) Zeng, G.; Yang, P.; Zheng, Z.; Feng, Q.; Cai, J.; Zhang, S.; Chen, Z. W. *Proteomics* **2005**, *5*, 4347–4353.
- (37) Yang, Z.; Yao, Z.; Li, G.; Fang, G.; Nie, H.; Liu, Z.; Zhou, X.; Chen, X.; Huang, S. *ACS Nano* **2012**, *6*, 205–211.
- (38) Matharu, Z.; Sumana, G.; Pandey, M. K.; Gupta, V.; Malhotra, B. D. *Thin Solid Films* **2009**, *518*, 719–723.